Laser control over the ultrafast Coulomb explosion of N_2^{2+} after Auger decay: A quantum-dynamics investigation

Athiya Mahmud Hanna,[1,2,*] Oriol Vendrell,[1,3,4,†] Abbas Ourmazd,[5] and Robin Santra[1,2,3,6]

[1]*Center for Free-Electron Laser Science, DESY, Notkestraße 85, D-22607 Hamburg, Germany*

[2]*Department of Chemistry, University of Hamburg, Martin-Luther-King-Platz 6, 20146 Hamburg, Germany*

[3]*Hamburg Centre for Ultrafast Imaging, Luruper Chaussee 149, D-22761 Hamburg, Germany*

[4]*Department of Physics and Astronomy, Aarhus University, Ny Munkegade 120, DK-8000 Aarhus C, Denmark*

[5]*Department of Physics, University of Wisconsin Milwaukee, 3135 N. Maryland Ave, Milwaukee, Wisconsin 53211, USA*

[6]*Department of Physics, University of Hamburg, Jungiusstraße 9, D-20355 Hamburg, Germany*

(Received 23 December 2016; published 24 April 2017)

By theoretical calculation, we demonstrate the possibility to control and partially suppress the Coulomb explosion of N_2 molecules after core-level photoionization by an x-ray laser and subsequent Auger decay. This is achieved by means of a femtosecond infrared laser pulse interacting with the N_2^{2+} dication produced by the x-ray pulse. Suppression of molecular fragmentation requires few-femtosecond IR pulses interacting with the system either during or shortly after the arrival of the x-ray pulse. The IR pulse suppresses fragmentation mostly by optically coupling the electronic routes to ultrafast molecular dissociation with electronic channels able to support long-lived vibrational resonances. The effect is strongly dependent on the orientation of the molecule with respect to the polarization axis of the IR field. Our calculations are motivated by x-ray pump–IR probe experiments performed at an x-ray free-electron laser [J. M. Glownia *et al.*, Opt. Express **18**, 17620 (2010)], where only enhancement of N_2^{2+} fragmentation as a function of the pump-probe delay time was reported. The opposite effect reported here becomes apparent when the various electronic channels are considered separately. In practice, this corresponds to a coincident measurement of the energy of the ejected Auger electron.

DOI: 10.1103/PhysRevA.95.043419

I. INTRODUCTION

Pump-probe experiments at free-electron lasers combining ultrashort x-ray and optical frequency pulses have the potential to unravel the inner workings of complex molecular systems with high temporal resolution and atomic or spatial specificity [1–4]. In such experiments, the relative timing of the x-ray and the optical pulses is one of the key issues and a nontrivial problem due to the very different nature of the two types of light source employed (cf. Ref. [4], and references therein).

Molecular nitrogen, especially in its dicationic state, is a well-characterized system extensively studied because of its metastable states [5–9]. So much so, that it is used as a benchmark for optimizing experimental parameters for pump-probe experiment at free-electron lasers [1,10–16]. The Auger decay of N_2 molecules has also been investigated extensively [12,17–21]. In Ref. [1] the dynamics of N_2 molecules following nitrogen $1s$ photoionization and the subsequent Auger decay were studied in an x-ray pump–IR probe setup at the Linac Coherent Light Source (LCLS). After $1s$ photoionization the monocationic system emits an Auger electron, resulting in a valence doubly ionized N_2^{2+}. It is well known that certain N_2^{2+} electronic states support vibrational resonances in which the molecular dication can stay bound for long times of up to seconds [5,22–25]. Measurements of the yield of N_2^{2+} as a function of pump-probe delay have shown that after x-ray absorption and Auger decay, the IR pulse enhances the fragmentation of N_2^{2+}, as evidenced by a clear yield reduction. Recently, a very sophisticated data analysis approach was applied to the same raw data, which was able to suppress most of the timing uncertainty of the original experiment, thus greatly increasing the accessible temporal range of pump-probe experiments at free-electron lasers [26].

Here, we investigate in detail the interaction of the IR pulse with the dicationic system, focusing on the effect of a short IR pulse on different electronic channels, either averaged as in typical experiments, or separately. A coincident measurement of the energy of the Auger electrons and the dications produced after the probe pulse can be realized to observe the effects of a short IR pulse on the N_2^{2+} system of specific electronic state as described here.

This paper is organized as follows. Section II summarizes the theory and computational methods used in this work, setting up the equation of motion for the system in Sec. II A, the potential energy curves (PECs) and their corresponding transition dipole moments (TDMs) in Sec. II B, and the quantum dynamics methods in Sec. II C. In Sec. III A, we discuss the Auger yields obtained in this work and the IR-free simulations. We then discuss the pump-probe simulations in Sec. III B. Finally, we summarize and conclude this work in Sec. IV.

II. THEORY AND COMPUTATIONAL METHODS

A. Model Hamiltonian

The various physical processes involved in the scenario under consideration here are illustrated in Fig. 1, namely, ionization of a $1s$ core electron by a short x-ray pulse $\epsilon_x(t-\tau_x)$ centered at time τ_x followed by Auger decay onto the manifold of doubly ionized valence states of N_2^{2+}. These states can interact with the infrared probe and control laser pulse $\epsilon_{\mathrm{IR}}(t-\tau_{\mathrm{IR}})$ centered at time τ_{IR}.

*athiya.m.hanna@cfel.de

†oriol.vendrell@phys.au.dk

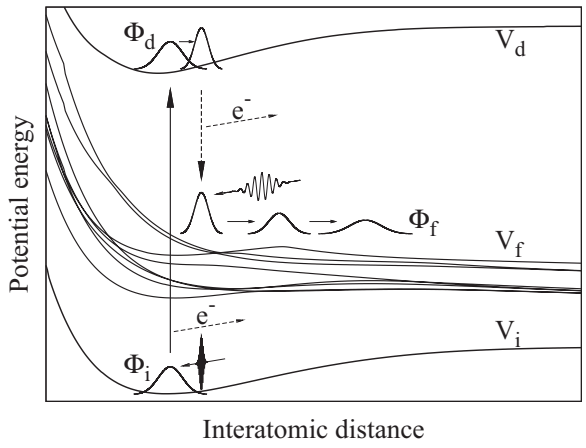

FIG. 1. Schematic diagram of the physical processes in the pump-probe experiment. The initial wave packet Φ_i is excited from the ground electronic state of N_2 into an intermediate, inner-shell-ionized electronic state by interaction with an x-ray pump pulse. The newly created Φ_d then propagates on the intermediate electronic state, and at the same time, decays to the final states, Φ_f, which interact with the IR probe pulse.

The total wave function for such a system can be expressed as

$$|\Psi(t)\rangle = |\Phi_i(t)\rangle|\psi_i^{(N)}\rangle + |\Phi_d(t)\rangle|\psi_d^{(N)}\rangle + \sum_f \int_0^\infty dE\,|\Phi_f(E,t)\rangle|\psi_f^{(N)}(E)\rangle, \quad (1)$$

where the Born-Oppenheimer separation of nuclear and electronic degrees of freedom is assumed and $|\Psi\rangle$, $|\Phi_{(i/d/f)}\rangle$, and $|\psi^{(N)}_{(i,d,f)}\rangle$ denote the total, nuclear, and electronic wave functions of the N electron system, respectively. We note that the outgoing Auger electron is part of the final state after Auger decay and therefore $|\Phi_f(E,t)\rangle$ and $|\psi_f^{(N)}(E)\rangle$ depend on its energy E [27]. The indices (i,d,f) denote the initial, decaying, and final states. The initial electronic state $|\psi_i^{(N)}\rangle$ corresponds to the ground state of neutral N_2. $|\psi_d^{(N)}\rangle$ is the intermediate electronic state consisting of $N_2{}^+$ generated by photoionization of a $1s$ core electron from N_2 to the continuum by interaction with the x-ray pulse and the ionized photoelectron. The final states $|\psi_f^{(N)}\rangle$ correspond to $N_2{}^{2+}$ after Auger decay has taken place, augmented by the energy normalized wave function of the emitted Auger and photoelectron.

For completeness we present here a short derivation of the equations of motion for the wave functions in Eq. (1). A detailed discussion is found in Ref. [27]. The total Hamiltonian of the system consists of the kinetic energy operator of the nuclei $\hat{T}_n$, the electronic Hamiltonian $\hat{H}_{\rm el}$, and the interaction term with external electric fields $\mathbf{E}(t)$ via the dipole operator $\hat{\mathbf{D}}$,

$$\hat{H}(t) = \hat{T}_n + \hat{H}_{\rm el} + \hat{\mathbf{D}}\cdot\mathbf{E}(t). \quad (2)$$

The total wave-function ansatz in Eq. (1) must fulfill the Schrödinger equation with the total Hamiltonian in Eq. (2),

$$i\frac{\partial}{\partial t}|\Psi(t)\rangle = \hat{H}(t)|\Psi(t)\rangle. \quad (3)$$

By taking the inner product of Eq. (3) with $\langle\psi_i^{(N)}|$, $\langle\psi_d^{(N)}|$, and $\langle\psi_f^{(N)}(E)|$, one obtains a set of coupled equations for the nuclear wave functions:

$$i\frac{\partial}{\partial t}|\Phi_i(t)\rangle = \hat{H}_i|\Phi_i(t)\rangle + \hat{F}_x^*(t)|\Phi_d(t)\rangle, \quad (4)$$

$$i\frac{\partial}{\partial t}|\Phi_d(t)\rangle = \hat{F}_x(t)|\Phi_i(t)\rangle + \hat{H}_d|\Phi_d(t)\rangle + \sum_f \int_0^\infty dE\,\hat{W}_f^\dagger(E)|\Phi_f(E,t)\rangle, \quad (5)$$

$$i\frac{\partial}{\partial t}|\Phi_f(E,t)\rangle = \hat{W}_f(E)|\Phi_d(t)\rangle + (\hat{H}_f + E)|\Phi_f(E,t)\rangle + \sum_{g\neq f}\hat{F}_{{\rm IR}\,fg}(t)|\Phi_g(E,t)\rangle, \quad (6)$$

where $\hat{H}_i$, $\hat{H}_d$, and $\hat{H}_f$ are the nuclear Hamiltonians acting on the nuclear part of the wave function corresponding to each electronic state and expressed as

$$\begin{aligned}\hat{H}_i &= \hat{T}_n + \hat{V}_i,\\ \hat{H}_d &= \hat{T}_n + \hat{V}_d,\\ \hat{H}_f &= \hat{T}_n + \hat{V}_f,\end{aligned} \quad (7)$$

with

$$\begin{aligned}\hat{V}_i &= \langle\psi_i^{(N)}|\hat{H}_{\rm el}|\psi_i^{(N)}\rangle,\\ \hat{V}_d &= \langle\psi_d^{(N)}|\hat{H}_{\rm el}|\psi_d^{(N)}\rangle,\\ \hat{V}_f &= \langle\psi_f^{(N)}|\hat{H}_{\rm el}|\psi_f^{(N)}\rangle.\end{aligned} \quad (8)$$

The operators $\hat{V}_{i/d/f}$ are matrix elements of the electronic Hamiltonian parametrized by the nuclear coordinates that act as potential energy operators in nuclear space. The Auger electron energy is reflected by a corresponding energy shift E of the final states Hamiltonian in Eq. (6) [27]. In essence, energy conservation is satisfied and thus Auger decay possible, only when the parameter E is of the order of the energy difference between the intermediate and final dicationic states. The transition operators $\hat{F}_x(t)$, $\hat{W}_f(E)$, and $\hat{F}_{{\rm IR}\,fg}(t)$ describe the x-ray interaction between the initial and the intermediate states, the Auger decay process from the intermediate to the final states, and the interaction of the optical laser with the final states of $N_2{}^{2+}$, respectively. Specifically, these terms are

$$\hat{F}_x(t) = \langle\psi_d^{(N)}|\hat{\mathbf{D}}|\psi_i^{(N)}\rangle\cdot\boldsymbol{\epsilon}_x\; A_x(t-\tau_x)\cos(\omega_x t), \quad (9)$$

$$\hat{W}_f(E) = \langle\psi_f^{(N)}(E)|\hat{H}_{\rm el}|\psi_d^{(N)}\rangle, \quad (10)$$

$$\hat{F}_{{\rm IR}\,fg}(t) = \langle\psi_f^{(N)}(E)|\hat{\mathbf{D}}|\psi_g^{(N)}(E)\rangle\cdot\boldsymbol{\epsilon}_{IR} \times A_{\rm IR}(t-\tau_{\rm IR})\cos[\omega_{\rm IR}(t-\tau_{\rm IR})-\phi_{\rm CEP}], \quad (11)$$

where $\boldsymbol{\epsilon}$ indicates a polarization direction and $A(t-\tau)$ corresponds to a pulse envelope with its maximum centered at time τ. The carrier-envelope phase $\phi_{\rm CEP}$ in Eq. (11) is taken to

be zero throughout the discussion, unless stated otherwise. In our model, the optical laser interacts only with the set of final states, which are separated by energies of the order of the IR photon energy [cf. Eq. (6)]. For the IR laser considered here, the ground electronic state of N_2 and the core-hole intermediate states have the nearest electronically excited states far off resonance [28]. Therefore, the interaction term with the optical laser does not enter Eqs. (4) and (5).

We now introduce an effective Hamiltonian $\hat{\mathcal{H}}_d$ for the intermediate-decaying state in order to effectively decouple its evolution in Eq. (5) from the evolution of the final states. Appendix A of Ref. [27] provides a detailed derivation leading to the effective Hamiltonian

$$\hat{\mathcal{H}}_d = \hat{H}_d - i\frac{\hat{\Gamma}}{2}, \tag{12}$$

where

$$\hat{\Gamma} = \sum_f \hat{\Gamma}_f, \qquad \hat{\Gamma}_f = 2\pi \hat{W}_f^\dagger \hat{W}_f. \tag{13}$$

At this point, the intermediate electronic state $|\psi_d\rangle$ still corresponds formally to the N-electron system, including the outgoing photoelectron. Since we are concerned only with the nuclear evolution in the intermediate state and not with the dynamics of the photoelectron, and since the x-ray photoionization process is considered to be fast and in the one-photon perturbative regime, the resulting set of working differential equations reads:

$$i\frac{\partial}{\partial t}|\Phi_d(t)\rangle = \hat{A}_x(t)|\Phi_i\rangle + \left(\hat{H}_d - i\frac{\hat{\Gamma}}{2}\right)|\Phi_d(t)\rangle, \tag{14}$$

$$i\frac{\partial}{\partial t}|\Phi_f(E,t)\rangle = \hat{W}_f|\Phi_d(t)\rangle + (\hat{H}_f + E)|\Phi_f(E,t)\rangle + \sum_{g\neq f}\hat{F}_{\mathrm{IR}\,fg}(t)|\Phi_g(E,t)\rangle. \tag{15}$$

The key assumption is that now the potential term in $\hat{H}_d = \hat{T}_n + \hat{V}_d$ in Eq. (14) is calculated for the core-ionized system consisting of $N-1$ electrons, thus implying a sudden ionization process [29] and the final states are similarly calculated for the $N-2$ electrons system. The $\hat{A}_x(t)$ operator is defined analogously to Eq. (9) but without the oscillatory carrier frequency part, which is removed through the rotating wave approximation [30]. Here, we consider eight final states, thus Eq. (15) together with Eq. (14) results in nine coupled differential equations that need to be numerically integrated.

B. Electronic structure calculations

Ab initio quantum chemistry calculations were carried out for the ground electronic state of N_2, the core-ionized $N_2^+(1s^{-1})$ state, as well as the final states of N_2^{2+} considered in this work, namely, $X\,{}^1\Sigma_g^+$, $2\,{}^1\Sigma_g^+$, $1\,{}^1\Delta_g$, $1\,{}^1\Pi_u$, $1\,{}^1\Pi_g$, $2\,{}^1\Pi_g$, $3\,{}^1\Pi_g$ and $1\,{}^1\Sigma_u^+$ electronic states. The corresponding PECs and transition dipole matrix elements required in the solution of Eqs. (14) and (15) were obtained on a grid for the interatomic distance coordinate between $1.6a_0$ (0.8467 Å) and $6.5a_0$ (3.4396 Å) divided into 520 grid points for the ground state of N_2 and the eight final states of N_2^{2+}, and 246 grid points for the PEC of the core-ionized state. The calculations employed the aug-cc-pVTZ atomic basis of Dunning [31]. The ground and excited electronic state wave functions and properties were calculated at the complete-active-space self-consistent-field level of theory using the MOLCAS package [32–34]. The active space used for the calculations of the N_2^{2+} consists of eight active electrons, the entire valence shell, and nine orbitals. The resulting PECs and TDMs are shown in Figs. 2 and 3, respectively.

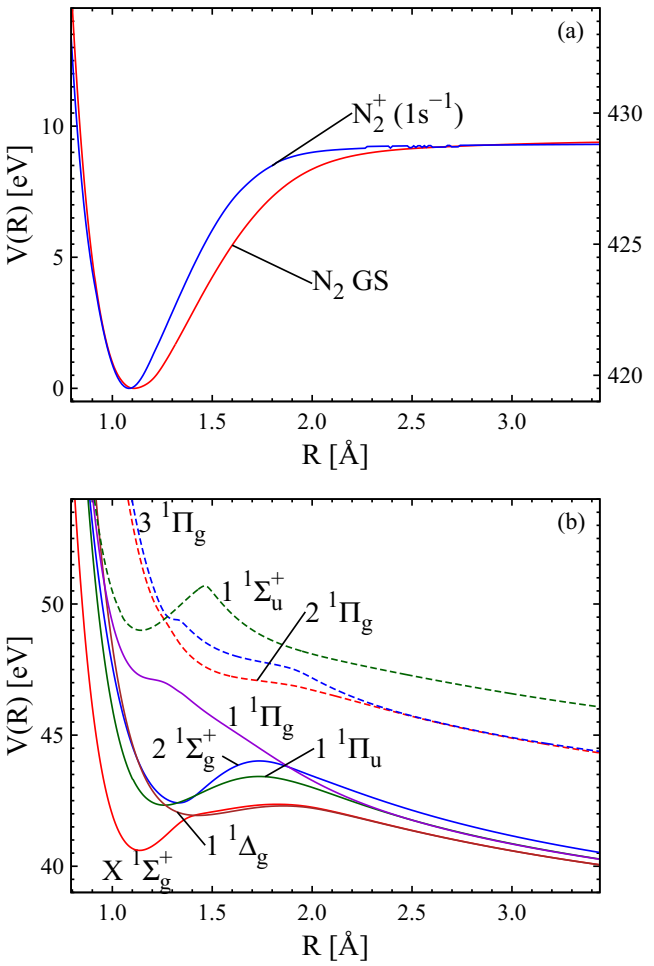

FIG. 2. PECs as functions of interatomic distance R. (a) shows PECs of the ground electronic state (GS) of N_2 (red line) and the intermediate state, $N_2^+(1s^{-1})$ (blue line). The potential energy axis of N_2 GS refers to the left-hand vertical y axis, while the $N_2^+(1s^{-1})$ state refers to the right-hand y axis. (b) shows PECs of the eight final states of N_2^{2+}. Energies are relative to the ground state minimum of N_2 (−2971.642 396 eV).

As shown in Fig. 2(b), there are five PECs with a local minimum that can accomodate metastable vibrational states, namely, $X\,{}^1\Sigma_g^+$, $1\,{}^1\Delta_g$, $2\,{}^1\Sigma_g^+$, $1\,{}^1\Pi_u$, and $1\,{}^1\Sigma_u^+$ states. Among those states, $1\,{}^1\Delta_g$ has a very shallow basin and its equilibrium distance is shifted away from the Franck-Condon region of N_2 in its ground vibrational state. Hence it is practically a dissociative state. The $2\,{}^1\Sigma_g^+$ and $1\,{}^1\Pi_u$ states have sufficiently deep minima to support some vibrational states but their equilibrium distances are displaced relative to the Franck-Condon region. The remaining $X\,{}^1\Sigma_g^+$ and $1\,{}^1\Sigma_u^+$ states, which also can support some vibrational states, are of particular importance in the nuclear dynamics because of their metastable

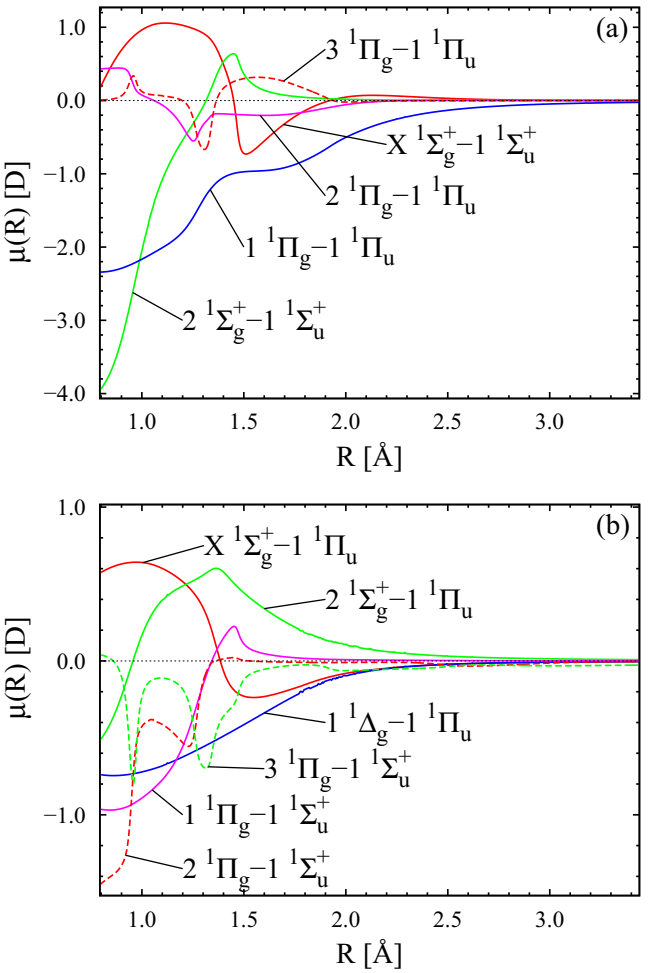

FIG. 3. Transition dipole moments for the eight final states of N_2^{2+} as functions of R. (a) shows parallel (z) components; (b) shows perpendicular (x,y) components.

features and matching Franck-Condon region as explained later in Sec. III.

Based on the coefficients of the configuration state functions, the major electronic configurations within the Franck-Condon region for the $X\,^1\Sigma_g^+$, $2\,^1\Sigma_g^+$, $1\,^1\Delta_g$, $1\,^1\Pi_u$, $1\,^1\Pi_g$, $2\,^1\Pi_g$, $3\,^1\Pi_g$, and $1\,^1\Sigma_u^+$ states are $3\sigma_g^{-2}$, $1\pi_u^{-2}3\sigma_g^{-0}$, $1\pi_u^{-2}3\sigma_g^{-0}$, $1\pi_u^{-1}3\sigma_g^{-1}$, $2\sigma_u^{-1}1\pi_u^{-1}3\sigma_g^{-0}$, $1\pi_u^{-2}3\sigma_g^{-1}1\pi_g^{+1}$, $1\pi_u^{-2}3\sigma_g^{-1}1\pi_g^{+1}$, and $1\pi_u^{-1}3\sigma_g^{-1}$, respectively. It can be seen that $p\pi$-type bonding is crucial in keeping the N_2^{2+} unfragmented with an equilibrium bond length as close as possible to N_2. This can be understood, since $p\pi$-type bonding has high electron density parallel to interatomic axes in a shorter bond length.

The PEC of the core-ionized $N_2^+(1s^{-1})$ state used here corresponds to the state of σ_u symmetry. The PEC of the σ_g state is practically parallel to the σ_u state and separated by about 100 meV [21,35] which is found to be very close to the lifetime broadening [8,21,35]. Since we used an experimental Auger rate Γ to characterize the decay process, it is immaterial for our model whether either or both of the states are considered.

C. Quantum dynamics

The N_2 molecule is described in two dimensions by the interatomic distance R and the polar angle θ between the molecular axis and the polarization axis of the IR field. The quantum dynamics of the two nuclear coordinates in the nine coupled electronic states, namely, Eqs. (14) and (15), are solved by the multiconfiguration time-dependent Hartree method [36–38]. The wave function along the R coordinate is represented on a Fourier grid with 240 equally spaced points between $1.6a_0$ (0.8467 Å) and $6.5a_0$ (3.4396 Å); the θ coordinate is described using a Legendre discrete variable representation on 60 grid points distributed in the interval $[0,\pi]$. We employ five time-dependent single-particle functions for each nuclear degree of freedom and use the so-called multiset formalism, in which each electronic state has its own set of time-dependent configurations [37].

In describing the decay process from the intermediate to the final states, we use the Auger-line assignment of Cryan *et al.* (Ref. [12]) to adjust the decay rates of our Hamiltonian. The transition operators describing Auger decay from the intermediate to the final states $\hat{W}_f$ are assumed to be constants proportional to the square root of the corresponding Auger yields of Ref. [12]. As for the total decay width of the intermediate state in Eq. (13), we use the experimental value of 103 meV from Ref. [8] which corresponds to the lifetime of 6.4 fs.

A complex absorbing potential (CAP) is used at the end of the R grid to avoid unphysical reflections of the dissociating part of the wave packets. The CAP is defined as

$$W = -i\eta\Theta(R-R_0)(R-R_0)^n, \tag{16}$$

where $\Theta(R-R_0)$ is the Heaviside step function and $R_0 = 4.5a_0$ (= 2.3813 Å), $\eta = 0.4218$ eV/a_0^n (= 1.5062 eV/Å^n), and $n = 2$ define the starting point, strength, and order of the CAP, respectively.

The population of unfragmented N_2^{2+} reaching the detector for a specific Auger energy E and IR pulse parameters is

$$\sigma^{N_2^{2+},\kappa}(E;\Delta_\tau,\mathbf{p}_\kappa) = \sum_f \sigma_f^{N_2^{2+},\kappa}(E;\Delta_\tau,\mathbf{p}_\kappa), \tag{17}$$

$$\sigma_f^{N_2^{2+},\kappa}(E;\Delta_\tau,\mathbf{p}_\kappa) = \langle\Phi_f(E,T_d)|\hat{\Theta}(R_b-R)|\Phi_f(E,T_d)\rangle, \tag{18}$$

where T_d is the time of arrival of the system at the detector and in practice the final time of the wave packet propagations. $R_b = 1.85$ Å is the interatomic distance for which all PECs at $R > R_b$ have a negative slope, i.e., the point of no return for the fragmentation of N_2^{2+} into two positively charged nitrogen atoms. We note that the $|\Phi_f(E,T_d)\rangle$ wave packets in Eq. (18) are propagated under the specific pulse parameters and delay time although these are not explicitly shown for the sake of notation clarity. $\Delta_\tau = \tau_{IR} - \tau_x$ is the pump-probe delay time and $\mathbf{p}_\kappa$ ($\kappa = 0,\ldots,6$) collects the different sets of IR pulse parameters listed in Table I, whereby $\kappa = 0$ corresponds to the case with no IR pulse and is therefore not listed. We considered different IR pulse realizations characterized by a photon energy of 1.5 eV [1]. The pulse envelope is assumed to be Gaussian and the six different pairs of optical intensity I_0, and pulse duration Δ_{IR} (which is defined as full width at

TABLE I. IR pulse parameters. The IR pulse number corresponds to the κ parameter in Eq. (17).

IR pulse	I_0 [10^{14} W cm^{-2}]	Δ_{IR} (FWHM) [fs]
IR 1	6.68	3.54
IR 2	4.48	5.30
IR 3	3.37	7.07
IR 4	2.24	10.61
IR 5	0.84	28.28
IR 6	0.56	42.43

half maximum of the pulse intensity) at fixed fluence are listed in Table I. Equations (14) and (15) were solved for varying Auger energies E ranging from 357.5 to 368.0 eV with an interval of 0.5 eV, plus an additional point at 366.8 eV for the simulations with various IR pulse parameters. The sum over final electronic state populations at a certain Auger energy E corresponds to the total Auger intensity and is given by

$$\sigma^A(E) = \sum_f \sigma_f^A(E), \tag{19}$$

$$\sigma_f^A(E) = \lim_{T\to\infty} \langle \Phi_f(E,T) | \Phi_f(E,T) \rangle \tag{20}$$

in which the Auger energy grid spacing is set to 0.2 eV to enable the comparison with the experimental data. The separate electronic state Auger intensity contributions $\sigma_f^A(E)$ are obtained in practice by removing the IR pulse and the CAPs from the Hamiltonian operator and propagating for a finite time until the populations become stationary.

III. RESULTS AND DISCUSSION

A. Auger yields

The PECs and electronic transition dipole operators are obtained by *ab initio* electronic structure calculations as described in Sec. II B. Also the coupling terms between decaying and final states $\hat{W}_f$ can be computed by *ab initio* means [39]. In this work, however, we take a simpler approach and adjust the coupling terms such that the channel populations $\sigma_f^A(E)$ calculated with our model match the Auger yield from the experimental results obtained by Cryan *et al.* (cf. Table 1 and Fig. 5 of Ref. [12] with Fig. 4). We assume that the coupling terms $\hat{W}_f$ and the total decay width of $N_2^+(1s^{-1})$ $\hat{\Gamma}$ are mere numbers independent of the nuclear coordinates [27], adjusted from the experimental values as described in Sec. II C. In essence, we employ a semiempirical Hamiltonian, which combines *ab initio* determined PECs and TDMs with decay parameters adjusted to experimental Auger decay measurements. The Auger spectrum obtained under this semiempirical model is shown in Fig. 4(a) and can be readily compared to Fig. 5 of Ref. [12]. We note, however, our approach does not, in general, conserve norm. In order to make the comparison fairly, we use these Auger intensities to normalize the populations. The calculated Auger yields are shown in Table II.

We are now in a position to solve Eqs. (14) and (15). Initially we concentrate on the freely decaying system without interaction with an IR laser. The quantity of interest is the unfragmented N_2^{2+} yield [Eq. (17)] as a function of the Auger electron energy for the different final electronic channels, which is shown in Fig. 4(b). Final states $1\,^1\Delta_g$ and $1\,^1\Pi_g$ lead to complete dissociation due to their repulsive PECs. States $2\,^1\Sigma_g^+$ and $1\,^1\Pi_u$ lead to partial dissociation although they can accommodate quasibound vibrational resonances in their

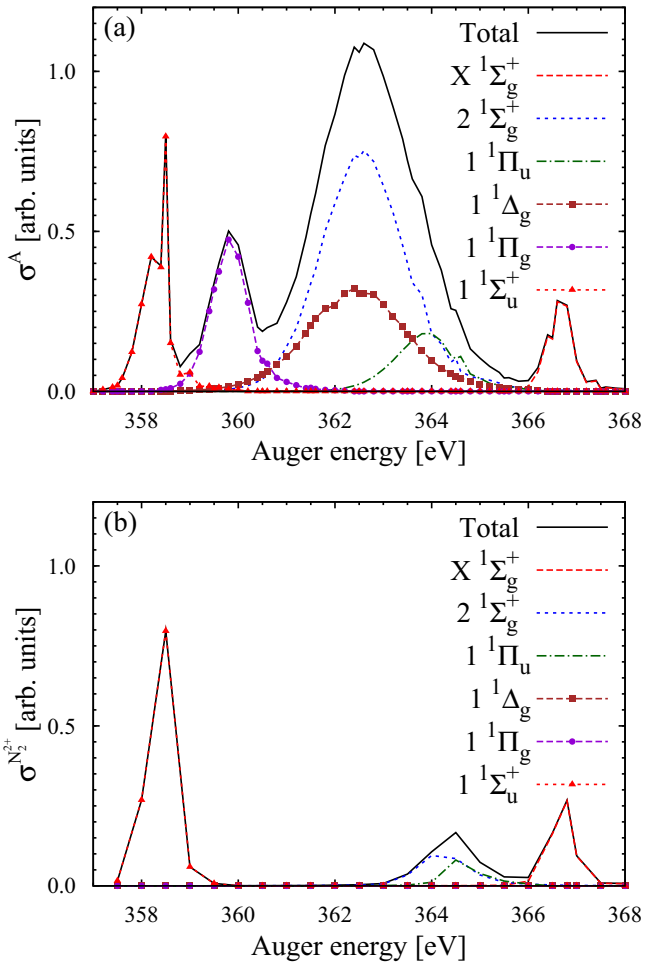

FIG. 4. (a) Auger yields calculated in this work; (b) population of unfragmented N_2^{2+} in IR-free simulations. The Auger yield calculations were performed with an energy grid spacing of 0.2 eV, while the IR-free simulations were done using 0.5 eV, as described in Sec. II C.

TABLE II. Calculated and experimental Auger yields from Ref. [12]. The empirical parameters of the Hamiltonian used in the calculations are adjusted to reproduce the corresponding experimental yield.

Final state	Calc. (%)	Expt. [12] (%)
$X\,^1\Sigma_g^+$	4.6	5.4 ± 0.5
$2\,^1\Sigma_g^+$	41.2	38 ± 1
$1\,^1\Pi_u$	7.4	7 ± 1
$1\,^1\Delta_g$	20.4	19 ± 1
$1\,^1\Pi_g$	11.9	11 ± 1
$1\,^1\Sigma_u^+$	14.5	9.4 ± 0.4

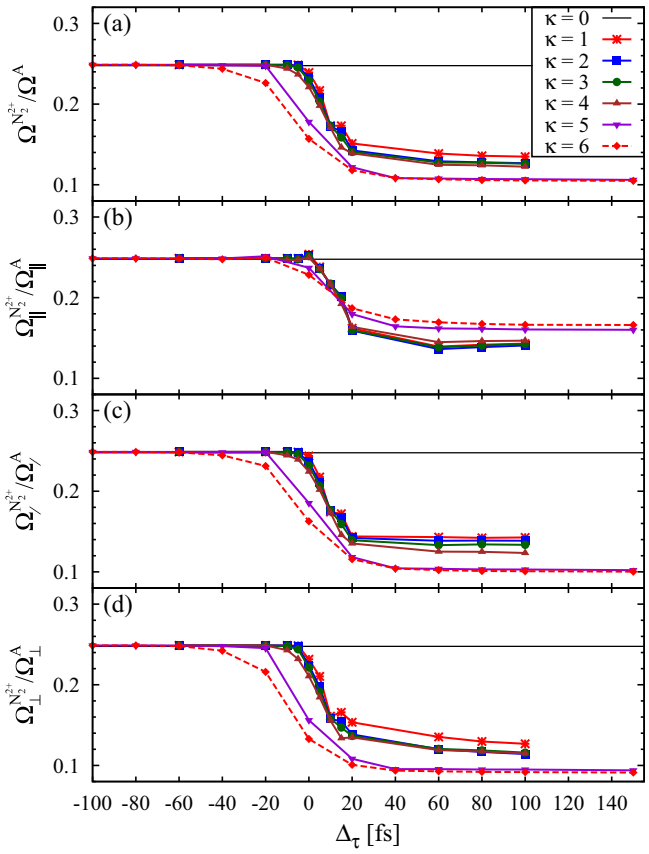

FIG. 5. The energy-integrated total $N_2{}^{2+}$ population in (a) the entire θ region $\Omega^{N_2{}^{2+},\kappa}$, (b) parallel region $\Omega_{\parallel}^{N_2{}^{2+},\kappa}$, (c) 45° region $\Omega_{\diagup}^{N_2{}^{2+},\kappa}$, and (d) perpendicular region $\Omega_{\perp}^{N_2{}^{2+},\kappa}$ for all IR pulses normalized by their corresponding energy-integrated Auger intensity.

PECs. This is because of the mismatch of equilibrium position and shape of the corresponding PECs with the intermediate state PEC, such that part of the vibrational wave packet can escape the potential energy well and lead to dissociation. In contrast, $X\,{}^1\Sigma_g^+$ and $1\,{}^1\Sigma_u^+$ are almost unfragmented within the time simulation window, since their equilibrium distance and PEC shape closely resemble those of the intermediate and initial electronic states, leading to a large population of deeply bound vibrational resonances of the corresponding final electronic states.

B. IR enhancement of $N_2{}^{2+}$ dissociation

The total $N_2{}^{2+}$ population after Auger decay integrated over the Auger electron energy

$$\Omega^{N_2{}^{2+},\kappa}(\Delta_\tau,\mathbf{p}_\kappa)=\int dE\,\sigma^{N_2{}^{2+},\kappa}(E;\Delta_\tau,\mathbf{p}_\kappa) \tag{21}$$

for the κth IR pulse parameters as a function of the delay time $\Delta_\tau=\tau_{\rm IR}-\tau_x$, normalized by the energy-integrated Auger spectrum

$$\Omega^A=\int dE\,\sigma^A(E), \tag{22}$$

is shown in Fig. 5(a). The effect of the IR pulse on the energy-integrated population is a reduction of the $N_2{}^{2+}$ yield, i.e., an enhancement of the molecular fragmentation. This effect is particularly pronounced for the longer IR pulses and also at the longer delay times. Essentially, the doubly ionized system quickly dissociates along the PECs of the $2\,{}^1\Sigma_g^+$, $1\,{}^1\Delta_g$, and $(1,2,3)\,{}^1\Pi_g$ states. States $1\,{}^1\Delta_g$ and $(1,2,3)^1\Pi_g$ practically feature repulsive PECs, whereas the $2\,{}^1\Sigma_g^+$ state has a local minimum at an interatomic distance of roughly 1.35 Å, as can be seen in Fig. 2. However, the PEC of the $2\,{}^1\Sigma_g^+$ state has a large repulsive slope in the Franck-Condon region which results mostly in dissociation (cf. Fig. 4). The shorter IR pulses $\kappa=1,\ldots,4$ characterized by pulse durations up to 10 fs do not display either enhancement or reduction of the $N_2{}^{2+}$ yield at short delay times $\Delta_\tau\approx 0$.

Analogously to the definition of Eq. (18), the $N_2{}^{2+}$ population can be defined for different orientations of the molecular axis with respect to the IR polarization direction,

$$\sigma_{f,(\parallel\diagup\perp)}^{N_2{}^{2+},\kappa}(E;\Delta_\tau,\mathbf{p}_\kappa)=\langle\Phi_f(E,T_d)|\hat{\mathcal{P}}_b\hat{\mathcal{P}}_{(\parallel\diagup\perp)}|\Phi_f(E,T_d)\rangle, \tag{23}$$

where the following definitions for the projection operators onto the R and θ coordinates are used:

$$\mathcal{P}_b=\hat{\Theta}(R_b-R), \tag{24}$$

$$\mathcal{P}_{(\parallel)}=\mathcal{P}_0^{30}+\mathcal{P}_{150}^{180}, \tag{25}$$

$$\mathcal{P}_{(\diagup)}=\mathcal{P}_{30}^{60}+\mathcal{P}_{120}^{150}, \tag{26}$$

$$\mathcal{P}_{(\perp)}=\mathcal{P}_{60}^{120}, \tag{27}$$

$$\mathcal{P}_{\theta_1}^{\theta_2}=\frac{\hat{\Theta}(\theta-\theta_1)\hat{\Theta}(\theta_2-\theta)}{2\pi(\cos\theta_1-\cos\theta_2)}. \tag{28}$$

The normalization factor in Eq. (28) corresponds to the spherical region between polar angles θ_1 and θ_2 after integration over the azimuthal angle, such that the resulting probabilities of different spherical regions can be directly compared. We have also used this orientation indexing ($\parallel$ / $\perp$) on integrated quantities Ω.

The energy-integrated $N_2{}^{2+}$ population of Eq. (23) is shown in Figs. 5(b)–5(d), where the effect of the different IR pulse parameters on molecules parallel, diagonal, and perpendicular to the polarization axis of the IR laser, respectively, can be seen. The energy-averaged $N_2{}^{2+}$ population is quite insensitive to the orientation of the molecules except for the fact that the longer IR pulses achieve a larger degree of fragmentation for molecules perpendicular to the IR polarization axis.

The molecular fragmentation of $N_2{}^{2+}$ caused by the interaction of the $N_2{}^{2+}$ with strong IR lasers has been the subject of experimental studies focusing on modification of the kinetic energy release of the fragments by the field [40,41]. Time-resolved experiments performed at LCLS based on x-ray pump–IR probe measurements found an enhancement of molecular fragmentation as a function of the pump-probe delay time [1], which is precisely the effect seen in Fig. 5(a) for different parameters of the laser pulse.

A deeper insight into the laser-driven ultrafast dynamics of metastable $N_2{}^{2+}$ is obtained by resolving the dication yield as a function of the Auger electron energy, which allows one to

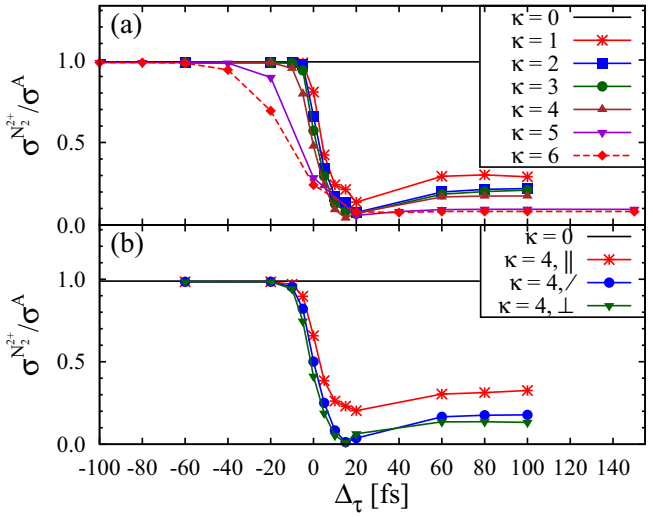

FIG. 6. Total N_2^{2+} population at Auger energy 358.5 eV for (a) the entire θ region $\sigma^{N_2^{2+},\kappa}$ for all IR pulses ($\kappa = 0,\ldots,6$), and (b) $\kappa = 4$ in parallel $\sigma_\parallel^{N_2^{2+},\kappa=4}$ (red line), $45^\circ\sigma_{\diagup}^{N_2^{2+},\kappa=4}$ (blue line), and perpendicular molecular orientation $\sigma_\perp^{N_2^{2+},\kappa=4}$ (green line) normalized by their corresponding Auger intensity σ^A.

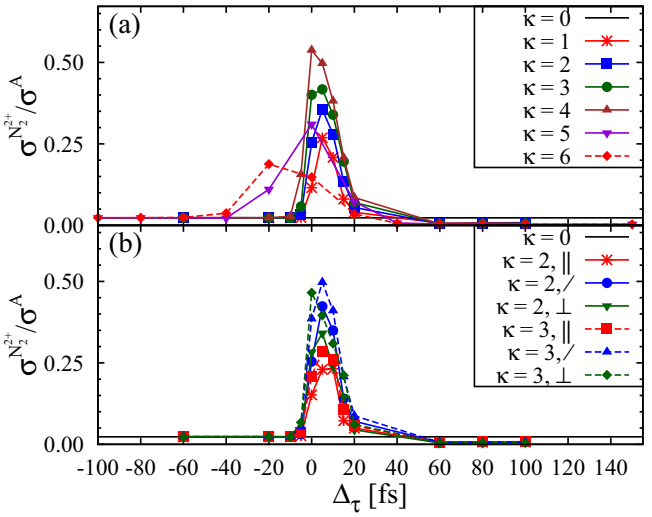

FIG. 7. Total N_2^{2+} population at Auger energy 359.5 eV for (a) the entire θ region $\sigma^{N_2^{2+},\kappa}$ for all IR pulses ($\kappa = 0,\ldots,6$), and (b) $\kappa = 2$ and $\kappa = 3$ in parallel $\sigma_\parallel^{N_2^{2+},\kappa=2,3}$ (red lines), $45^\circ\sigma_{\diagup}^{N_2^{2+},\kappa=2,3}$ (blue lines), and perpendicular molecular orientation $\sigma_\perp^{N_2^{2+},\kappa=2,3}$ (green lines) normalized by their corresponding Auger intensity σ^A.

disentangle the response of the system in the different final electronic states. To the best of our knowledge, such type of measurements have not been reported to date. In the following we discuss the N_2^{2+} yield for various Auger electron energies and as a function of molecular orientation.

At Auger energy 358.5 eV shown in Fig. 6, one sees that the IR pulse enhances the dissociation of N_2^{2+} for all pulse durations relative to the IR-free case. This is no surprise after inspecting the PEC of the $1\,^1\Sigma_u^+$ state, which has a deep metastable potential energy well where population remains trapped after Auger decay, and which is almost exclusively populated at this Auger energy. The incoming IR pulse with a 1.5 eV central photon energy resonantly transfers population to the dissociative $1\,^1\Pi_g$ state since the energy difference between those two states is very close to 1.5 eV. Our calculation at this Auger energy also shows that the IR pulse also partially populates the dissociative $2\,^1\Pi_g$ state.

The $1\,^1\Sigma_u^+ \rightarrow (1,2)\,^1\Pi_g$ transitions originate from the perpendicular components (μ_x,μ_y) of transition dipole moment between both electronic states. Because of this, the enhancement of N_2^{2+} fragmentation is more efficient if the molecule is found perpendicular to the IR laser polarization, as can be appreciated in Fig. 6(b). Note that the enhancement of fragmentation is also seen for the zero degrees case because of the finite θ range considered around each main orientation.

Figure 7 shows the N_2^{2+} population for an Auger energy of 359.5 eV, which is complementary to the 358.5 eV case discussed above. Now, N_2^{2+} dications have mostly Auger decayed into the $1\,^1\Pi_g$ final state, which is strongly dissociative. This means that only a short IR pulse interacting with the dication before it leaves the Franck-Condon region in about 10–20 fs is able to stabilize the otherwise Coulomb exploding system by transferring population to the metastable $1\,^1\Sigma_u^+$ state. Once the wave packet has propagated to longer interatomic distances than about 1.5 Å, the IR pulse is not able to trap the fragmenting N_2^{2+} system anymore. The largest effect hence occurs for the shorter pulses, and the stabilization effect is almost inexistent for pump-probe delays larger than about 20 fs. As before, at this Auger energy the dominant IR-induced transition is $1\,^1\Pi_g \rightarrow 1\,^1\Sigma_u^+$, which is allowed only for photons polarized perpendicular to the molecular axis. However, the 45° case when the system experiences more than half of the IR pulse [i.e., the delay time is larger than zero, as seen in Fig. 7(b)] displays the higher stabilization effect compared to the perpendicular case. This inversion is caused by the large laser intensity, which at 90° is able to induce more than half a Rabi cycle, therefore reducing the final amount of population transferred to the metastable state. This effect is observed especially for the shorter pulses and indicates that an IR laser with a slightly smaller intensity than assumed here and than the one used in the experiments of Ref. [1] would be sufficient to observe this inversion effect.

At an Auger energy of 362.5 eV as shown in Figure 8, primarily two final states are populated by the Auger decay process, namely, $2\,^1\Sigma_g^+$ and $1\,^1\Delta_g$. Without the IR pulse (or at long negative or positive delay times), N_2^{2+} almost completely fragments because the potential energy within the Franck-Condon region is higher than the $2\,^1\Sigma_g^+$ energy barrier toward dissociation, whereas $1\,^1\Delta_g$ is practically a dissociative state. In this energy range the IR pulse can only suppress the fragmentation process mostly through two 2-photon pathways: $2\,^1\Sigma_g^+ \rightarrow 1\,^1\Pi_u$ and $1\,^1\Delta_g \rightarrow 1\,^1\Pi_u$ then followed by $1\,^1\Pi_u \rightarrow X\,^1\Sigma_g^+$, with $1\,^1\Pi_u$ serving as a bridge state. The two consecutive transitions are both related to perpendicular components of the TDMs. Shorter IR pulses have a higher optical intensity and lead with higher probability to these two-photon pathways, thus resulting in a stronger suppression of dissociation at this Auger energy. The same argument also applies at Auger energy of 359.5 eV in Fig. 7.

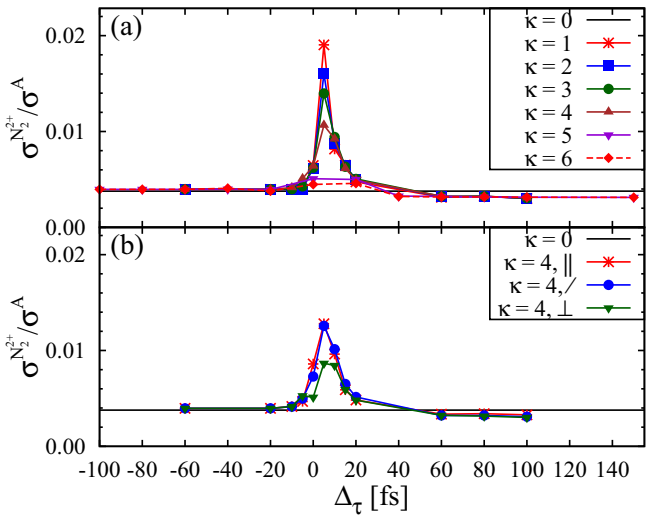

FIG. 8. Total N_2^{2+} population at Auger energy 362.5 eV for (a) the entire θ region $\sigma^{N_2^{2+},\kappa}$ for all IR pulses ($\kappa = 0,\ldots,6$), and (b) $\kappa = 4$ in parallel $\sigma_\parallel^{N_2^{2+},\kappa=4}$ (red line), 45° $\sigma_/^{N_2^{2+},\kappa=4}$ (blue line), and perpendicular molecular orientation $\sigma_\perp^{N_2^{2+},\kappa=4}$ (green line) normalized by their corresponding Auger intensity σ^A.

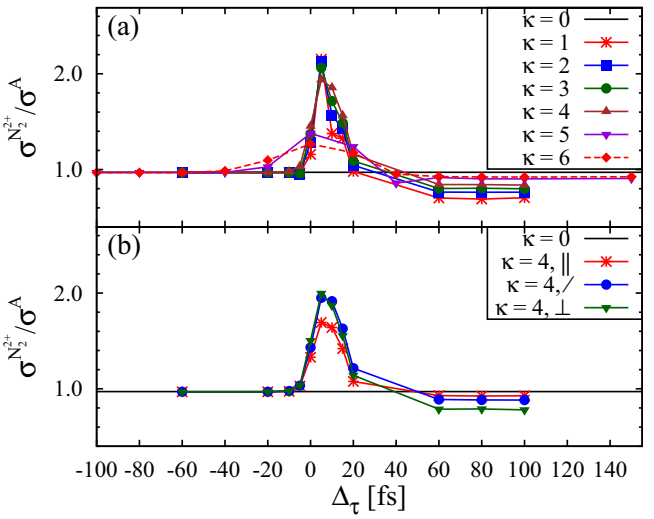

FIG. 9. Total N_2^{2+} population at Auger energy 367.0 eV for (a) the entire θ region $\sigma^{N_2^{2+},\kappa}$ for all IR pulses ($\kappa = 0,\ldots,6$), and (b) $\kappa = 4$ in parallel $\sigma_\parallel^{N_2^{2+},\kappa=4}$ (red line), 45° $\sigma_/^{N_2^{2+},\kappa=4}$ (blue line), and perpendicular molecular orientation $\sigma_\perp^{N_2^{2+},\kappa=4}$ (green line) normalized by their corresponding Auger intensity σ^A.

However, at this latter Auger energy, the two-photon pathways imply a return to the dissociative (1,2) $^1\Pi_g$ states.

Finally we consider the case in which the Auger electron is emitted with an energy of 367.0 eV. We deliberately discuss this case where the IR-free yield is about 50% lower than at 366.8 eV, the Auger energy of the peak corresponding to the $X\,^1\Sigma_g^+$ channel (cf. Fig. 4). At 367.0 eV all Auger yield corresponds exclusively to the $X\,^1\Sigma_g^+$ channel and all dications produced stay trapped in low-energy vibrational resonances of this electronic state. However, one can clearly identify an enhancement of the N_2^{2+} yield for IR pulses overlapping with the x-ray pump pulse as depicted in Fig. 9. As expected, negative delay times have no effect on the N_2^{2+} yield and positive delay times beyond about 40 fs have the effect of slightly depleting the N_2^{2+} population by either vibrational or electronic excitation into dissociative states.

The enhancement around zero-delay time has to be understood as a genuine strong-field effect, since at this Auger energy no other more energetic electronic channels are populated, from which population could be transferred to the $X\,^1\Sigma_g^+$ state. The strong IR pulse is in resonance with the $X\,^1\Sigma_g^+ \rightarrow 1\,^1\Pi_u$ transition and the resulting dressed states naturally split during the IR pulse [42,43], effectively shifting the $X\,^1\Sigma_g^+$ final electronic state down to a lower energy only during the IR pulse and, as a consequence, leading to a shift of the energy of the Auger electron for short time delays. The same type of strong coupling by an IR laser is known to lead to bond softening [44].

As the shortest IR pulse ($\kappa = 1$) consists of only a few cycles, we address here the role of the carrier-envelope phase $\phi_{\rm CEP}$ in controlling the dynamics of the dicationic system [cf. Eq. (11)]. The carrier-envelope phase for $\kappa = 1$ is varied over the interval $[0, \frac{\pi}{2}]$ with an interval of $\frac{\pi}{20}$ for a 5 fs delay time and the enhancement or suppression of the molecular dication population is shown in Fig. 10 relative to the case $\phi_{\rm CEP} = 0$ at different Auger energies. We find that a variation of 15% in the suppression of dissociation occurs at a phase of $\frac{2\pi}{5}$ for Auger energy 359.5 eV. A 6% of enhancement of dissociation can be seen at Auger energy of 362.5 eV with $\phi_{\rm CEP}$ close to $\frac{\pi}{4}$. At other Auger energies, and for the Auger energy-integrated yield, the variations with respect to $\phi_{\rm CEP} = 0$ are smaller than 3%.

The fragmentation and stabilization of N_2^{2+} by an IR pulse can also be viewed as chemical bonding rearrangement. As noted before, the $p\pi$-type bonding is important in N-N

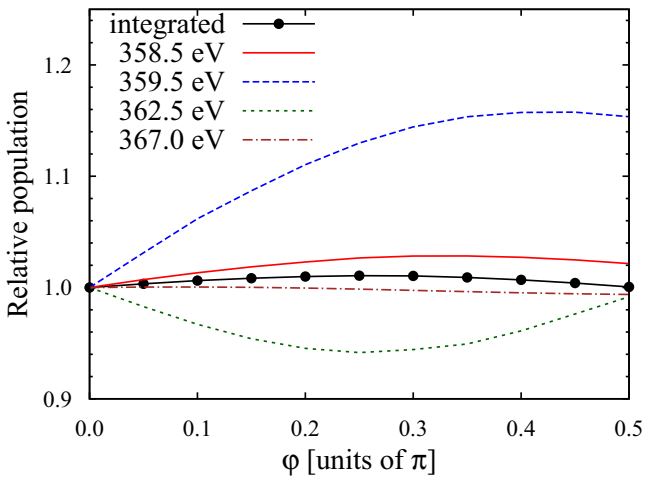

FIG. 10. Relative N_2^{2+} yield as a function of carrier-envelope phase $\phi_{\rm CEP}$ for the shortest IR pulse ($\kappa = 1$) and delay time of 5 fs. The energy-integrated yield $\frac{\Omega^{N_2^{2+}}(\phi)}{\Omega^{N_2^{2+}}(\phi=0)}$ is shown together with the corresponding differential quantities $\frac{\sigma^{N_2^{2+}}(\phi)}{\sigma^{N_2^{2+}}(\phi=0)}$ at Auger energies 358.5, 359.5, 362.5, and 367.0 eV.

bonding of N_2^{2+}. The incoming IR pulse can either restore the $p\pi$ bonding, thus resulting in stabilization, or break it, resulting in fragmentation of N_2^{2+}. At Auger energy of 358.5 eV the IR pulses break the $p\pi$ bonding of N_2^{2+} causing the enhancement of fragmentation, while at Auger energies of 359.5 and 362.5 eV the IR pulses restore the $p\pi$ bonding within N_2^{2+} resulting in the suppression of fragmentation.

IV. CONCLUSIONS

We have performed x-ray–IR pump-probe quantum dynamical simulations of N_2 molecules. After photoionization by the x-ray pulse the $N_2^+(1s^{-1})$ system decays through emission of an Auger electron resulting in N_2^{2+} with two electron vacancies in the valence shell. We explicitly treated eight final N_2^{2+} states, namely, $X\ ^1\Sigma_g^+$, $2\ ^1\Sigma_g^+$, $1\ ^1\Pi_u$, $1\ ^1\Delta_g$, $1\ ^1\Pi_g$, $2\ ^1\Pi_g$, $3\ ^1\Pi_g$, and $1\ ^1\Sigma_u^+$ and one $N_2^+(1s^{-1})$ state as the intermediate-decaying state, whereby some of the PECs of these electronic states support long-lived vibrational resonances of the N_2^{2+} dication [5,22–25]. X-ray pump–IR probe experiments conducted at the LCLS free-electron laser had shown that an IR pulse delayed with respect to the x-ray pump has the ability to enhance the dissociation out of such resonant vibrational states [1]. In those experiments the Auger electron energy and therefore the final electronic channel of the dication remained undetected.

When summing over all electronic channels our results are qualitatively in agreement with the enhancement of dissociation of N_2^{2+} reported in Ref. [1] (cf. Fig. 5 with Fig. 5 in Ref. [1]). On top of that we demonstrate stabilization of the N_2^{2+} dication by the IR laser when the laser pulse is short and interacts with the system during or shortly after the interaction with the x-ray pulse. This inverse effect is found for the electronic channels that lead to very fast dissociation and requires that the IR laser couple such electronic states with electronic states that support vibrational resonances before the fragmentation process has taken place. In particular, we have examined three regions of the Auger energy spectrum in which this effect could be measured, namely, 359.5, 362.5, and 367.0 eV. At Auger energies of 359.5 and 362.5 eV the corresponding final electronic states $1\ ^1\Pi_g$ and $2\ ^1\Sigma_g^+$ have strongly dissociative PECs. Stabilization thus requires that the IR pulse has a duration of at most a few tens of femtoseconds and interact with the system before the onset of fragmentation, which also takes only a few tens of femtoseconds to complete. At 367.0 eV only the ground electronic state $X\ ^1\Sigma_g^+$ becomes populated, which supports long-lived vibrational resonances. The intensity maximum of the Auger spectrum for this channel in the absence of the IR pulse is at about 366.5 eV. The presence of the IR pulse *during* the Auger decay has the effect of changing the energy of the final state, effectively dressing it in the presence of the IR photon. This results in an enhancement of the N_2^{2+} dication population as a function of the pump-probe delay, which however has now a different physical origin than in the case where highly dissociative electronic states become populated. Since all electronic transitions involved are related to (μ_x, μ_y) TDMs where the z axis corresponds to the molecular axis, they are most effective for systems perpendicularly oriented with respect to the polarization axis of the IR laser field. Examination of the effect of the carrier-envelope phase of the shortest pulse at 5 fs delay time reveals additional 15% suppression of the dissociation effect at 359.5 eV, and enhancement of dissociation of about 6% at 362.5 eV.

These results demonstrate the possibility of control over a Coulomb explosion process following irradiation with an x-ray pulse, and provide a theoretical benchmark for future x-ray–optical pump-probe experiments at free-electron lasers.

ACKNOWLEDGMENT

The work conducted by A.O. was supported by the U.S. Department of Energy, Office of Science, Basic Energy Sciences under award DE-SC0002164.

[1] J. M. Glownia, J. Cryan, J. Andreasson, A. Belkacem, N. Berrah, C. I. Blaga, C. Bostedt, J. Bozek, L. F. DiMauro, L. Fang *et al.*, Opt. Express **18**, 17620 (2010).

[2] V. S. Petrović, M. Siano, J. L. White, N. Berrah, C. Bostedt, J. D. Bozek, D. Broege, M. Chalfin, R. N. Coffee, J. Cryan *et al.*, Phys. Rev. Lett. **108**, 253006 (2012).

[3] B. K. McFarland, J. P. Farrell, S. Miyabe, F. Tarantelli, A. Aguilar, N. Berrah, C. Bostedt, J. D. Bozek, P. H. Bucksbaum, J. C. Castagna *et al.*, Nat. Commun. **5**, 4235 (2014).

[4] A. Rudenko and D. Rolles, J. Electron Spectrosc. Relat. Phenom. **204**, 228 (2015).

[5] R. W. Wetmore and R. K. Boyd, J. Phys. Chem. **90**, 5540 (1986).

[6] G. Dawber, A. G. McConkey, L. Avaldi, M. A. MacDonald, G. C. King, and R. I. Hall, J. Phys. B **27**, 2191 (1994).

[7] P. R. Taylor and H. Partridge, J. Phys. Chem. **91**, 6148 (1987).

[8] B. Kempgens, A. Kivimäki, M. Neeb, H. M. Köppe, A. M. Bradshaw, and J. Feldhaus, J. Phys. B **29**, 5389 (1996).

[9] W. Jiang, Y. G. Khait, and M. R. Hoffmann, J. Chem. Phys. **127**, 164308 (2007).

[10] J. P. Cryan, J. M. Glownia, J. Andreasson, A. Belkacem, N. Berrah, C. I. Blaga, C. Bostedt, J. Bozek, C. Buth, L. F. DiMauro *et al.*, Phys. Rev. Lett. **105**, 083004 (2010).

[11] M. Hoener, L. Fang, O. Kornilov, O. Gessner, S. T. Pratt, M. Gühr, E. P. Kanter, C. Blaga, C. Bostedt, J. D. Bozek *et al.*, Phys. Rev. Lett. **104**, 253002 (2010).

[12] J. P. Cryan, J. M. Glownia, J. Andreasson, A. Belkacem, N. Berrah, C. I. Blaga, C. Bostedt, J. Bozek, N. A. Cherepkov, L. F. DiMauro *et al.*, J. Phys. B **45**, 055601 (2012).

[13] H. Fukuzawa, K. Motomura, X.-J. Liu, G. Prümper, M. Okunishi, K. Ueda, N. Saito, H. Iwayama, K. Nagaya, M. Yao, M. Nagasono, A. Higashiya, M. Yabashi, T. Ishikawa, H. Ohashi, and H. Kimura, J. Phys. B **42**, 181001 (2009).

[14] A. Föhlisch, M. Nagasono, M. Deppe, E. Suljoti, F. Hennies, A. Pietzsch, and W. Wurth, Phys. Rev. A **76**, 013411 (2007).

[15] A. A. Sorokin, S. V. Bobashev, K. Tiedtke, and M. Richter, J. Phys. B **39**, L299 (2006).

[16] M. Magrakvelidze, O. Herrwerth, Y. H. Jiang, A. Rudenko, M. Kurka, L. Foucar, K. U. Kühnel, M. Kübel, N. G. Johnson, C. D. Schröter, S. Düsterer, R. Treusch, M. Lezius, I. Ben-Itzhak, R.

Moshammer, J. Ullrich, M. F. Kling, and U. Thumm, Phys. Rev. A **86**, 013415 (2012).
[17] W. E. Moddeman, T. A. Carlson, M. O. Krause, B. P. Pullen, W. E. Bull, and G. K. Schweitzer, J. Chem. Phys. **55**, 2317 (1971).
[18] H. Ågren, J. Chem. Phys. **75**, 1267 (1981).
[19] S. Svensson, A. N. D. Brito, M. P. Keane, N. Correia, L. Karlsson, C.-M. Liegener, and H. Agren, J. Phys. B **25**, 135 (1992).
[20] G. Víkor, S. Ricz, L. Tóth, B. Sulik, J. Végh, Á. Kövér, and L. Kövér, Nucl. Instrum. Methods Phys. Res., Sect. B **124**, 393 (1997).
[21] S. L. Sorensen, C. Miron, R. Feifel, M. N. Piancastelli, O. Björneholm, and S. Svensson, Chem. Phys. Lett. **456**, 1 (2008).
[22] B. J. Olsson, G. Kindvall, and M. Larsson, J. Chem. Phys. **88**, 7501 (1988).
[23] T. E. Masters and P. J. Sarre, J. Chem. Soc. Faraday Trans. **86**, 2005 (1990).
[24] P. C. Cosby, R. Möller, and H. Helm, Phys. Rev. A **28**, 766 (1983).
[25] P. A. Martin, F. R. Bennett, and J. P. Maier, J. Chem. Phys. **100**, 4766 (1994).
[26] R. Fung, A. M. Hanna, O. Vendrell, S. Ramakrishna, T. Seideman, R. Santra, and A. Ourmazd, Nature (London) **532**, 471 (2016).
[27] E. Pahl, H.-D. Meyer, and L. S. Cederbaum, Z. Phys. D **38**, 215 (1996).
[28] F. R. Gilmore, J. Quant. Spectrosc. Radiat. Transfer **5**, 369 (1965).
[29] B. T. Pickup, Chem. Phys. **19**, 193 (1977).
[30] E. T. Jaynes and F. W. Cummings, Proc. IEEE **51**, 89 (1963).
[31] T. H. Dunning, Jr., J. Chem. Phys. **90**, 1007 (1989).
[32] G. Karlström, R. Lindh, P.-Å. Malmqvist, B. O. Roos, U. Ryde, V. Veryazov, P.-O. Widmark, M. Cossi, B. Schimmelpfennig, P. Neogrady, and L. Seijo, Comput. Mater. Sci. **28**, 222 (2003).
[33] V. Veryazov, P.-O. Widmark, L. Serrano-Andrés, R. Lindh, and B. O. Roos, Int. J. Quantum Chem. **100**, 626 (2004).
[34] F. Aquilante, L. De Vico, N. Ferré, G. Ghigo, P.-å. Malmqvist, P. Neogrády, T. B. Pedersen, M. Pitoák, M. Reiher, B. O. Roos, L. Serrano-Andrés, M. Urban, V. Veryazov, and R. Lindh, J. Comput. Chem. **31**, 224 (2010).
[35] U. Hergenhahn, O. Kugeler, A. Rdel, E. E. Rennie, and A. M. Bradshaw, J. Phys. Chem. A **105**, 5704 (2001).
[36] H. D. Meyer, U. Manthe, and L. S. Cederbaum, Chem. Phys. Lett. **165**, 73 (1990).
[37] M. H. Beck, A. Jäckle, G. A. Worth, and H. D. Meyer, Phys. Rep. **324**, 1 (2000).
[38] H.-D. Meyer and G. A. Worth, Theor. Chem. Acc. **109**, 251 (2003).
[39] J. Craigie, A. Hammad, B. Cooper, and V. Averbukh, J. Chem. Phys. **141**, 014105 (2014).
[40] R. N. Coffee, L. Fang, and G. N. Gibson, Phys. Rev. A **73**, 043417 (2006).
[41] W. Lai, L. Pei, and C. Guo, Phys. Rev. A **84**, 043413 (2011).
[42] D. J. Tannor, *Introduction to Quantum Mechanics: A Time-Dependent Perspective* (University Science Books, Sausalito, California, 2007), p. 479.
[43] P. R. Berman, Phys. Rev. A **53**, 2627 (1996).
[44] P. H. Bucksbaum, A. Zavriyev, H. G. Muller, and D. W. Schumacher, Phys. Rev. Lett. **64**, 1883 (1990).